Soft Matter

Cite this: *Soft Matter*, 2011, **7**, 9444

www.rsc.org/softmatter

PAPER

Extensional rheology of DNA suspensions in microfluidic devices†

Gabriel Juarez and Paulo E. Arratia*

Received 25th February 2011, Accepted 27th July 2011
DOI: 10.1039/c1sm05347g

Newtonian liquids that contain even small amounts (~ppm) of flexible polymers can exhibit viscoelastic behavior in extensional flows. Here, the effects of the presence of DNA molecules in viscous fluids on the dynamics of filament thinning and drop breakup are investigated experimentally in a cross-slot microchannel. Both bulk flow and single molecule experiments are presented. Suspensions of DNA molecules of different molecular weights (MW) are used, namely λ-DNA (MW = 3×10^7) and T4 DNA (MW = 1×10^8). Results of both dilute ($c/c^* = 0.5$) and semi-dilute ($c/c^* = 1$) suspensions are compared to those of a viscous, Newtonian liquid. Results show that the dynamics of the high MW, semi-dilute suspension of T4 DNA are similar to viscoelastic fluids such as slow, exponential decay of the fluid thread and beads-on-a-string morphology. The exponential decay rate of the filament thickness is used to measure the steady extensional viscosity of all fluids. We find that the semi-dilute T4 DNA suspension exhibits extensional strain rate thinning extensional viscosity, while for all other fluids the extensional viscosity is independent of strain rate. Direct visualization of fluorescently labeled λ-DNA molecules using high-speed imaging shows that the strong flow in the thinning fluid threads provide sufficient forces to stretch the majority of DNA molecules away from their equilibrium coiled state. The distribution of molecular stretch lengths, however, is very heterogeneous due to molecular individualism and initial conditions.

1. Introduction

Many biological processes, including protein folding and gene transcription, are affected by the mechanical and dynamical properties of bio-polymers. For example, the rigidity of actin and myosin in muscles provide the structure that maintains the cell shape,[1] while the flexibility of DNA enables it to undergo a drastic change in conformation from an elongated state to a very compact and highly ordered toroidal structure during DNA condensation.[2] The dynamics of bio-polymers in fluids has attracted much attention,[3–7] in particular the flow of DNA suspensions in lab-on-chip devices for applications that include genome mapping[8–10] and DNA separation,[11,12] as well as for the study of polymer physics.[13–19] Understanding the rheological and flow properties of DNA suspensions are of much practical importance and can lead to better insights into the dynamics of macromolecules.

The flow of liquids containing DNA molecules in small scale devices ($L < 10^{-6}$ m) can often display non-linear flow behavior.[20,21] Mechanical stresses of DNA fluids are history dependent and depend on a characteristic time λ that in dilute solutions is proportional to the relaxation time of a single DNA molecule. In semi-dilute solutions, λ also depends on molecular interactions. These stresses grow non-linearly with strain rate and can dramatically change the flow behavior. For example, it is known that even at low Reynolds numbers (Re), DNA molecules can be stretched to full length in regions of high-velocity gradients.[22–26] Here, $\mathrm{Re} = \rho VL/\mu$, where V and L are the characteristic fluid velocity and length scale and ρ and μ are the fluid density and viscosity, respectively. In addition, viscoelastic effects, which can be quantified by the elasticity number $El = \lambda\mu/(\rho L^2)$, scale inversely with the square of the device length scale and are likely to be accentuated in lab-on-chip devices.

Much effort has been devoted to characterizing the rheological properties of DNA suspensions in shear flows.[27–29] The extensional viscosity η_e of such fluids, on the other hand, have not been investigated in detail even though many lab-on-chip operations rely heavily on extensional flows to stretch DNA molecules for genome mapping, for example. For Newtonian fluids, the extensional viscosity is equal to three times its shear viscosity such that $\eta_e = 3\mu$. For complex fluids, including polymeric fluids, the value of η_e can be orders of magnitude larger than its shear viscosity.[30,31] A common way to measure η_e is to analyze the thinning and the subsequent breakup of an initially stable fluid thread in filament stretching[32,33] and capillary breakup[34–37] rheometers, jet breakup,[38,39] and drop pinch-off.[40–42] In particular, the capillary breakup extensional rheometer (CaBER) has been shown to provide reliable measurements of the transient extensional viscosity.[34,43] Recently, it has been shown that similar measurements can be made in a flow focusing microfluidic

Department of Mechanical Engineering and Applied Mechanics, University of Pennsylvania, Philadelphia, PA 19104, USA. E-mail: parratia@seas.upenn.edu

† Electronic supplementary information (ESI) available. See DOI: 10.1039/c1sm05347g

device[44,45] in which the steady extensional viscosity is measured as a function of extensional strain rate. One of the advantages of the microfluidic device methods is that it allows for a simultaneous measurements of the bulk flow behavior and visualization of the DNA molecules in the fluid thread.

In this article, we investigate the fluid thinning and drop breakup process of DNA suspensions in a cross-slot microchannel. DNA suspensions are of particular interest because they can be used to study the dynamics of single (bio)-polymers by direct visualization,[13,14] and they also serve as archetypes of viscoelastic fluids. Here, we present for the first time, single molecule measurements inside a thinning fluid filament. Double-stranded DNA molecules of different molecular weights, namely λ-phage DNA and T4 DNA, are used. Results for the DNA suspensions are compared to those for Newtonian fluids of same shear-viscosity. We find that the DNA suspensions display features during the thinning and breaking process that are typical to viscoelastic fluids, including long filaments and beads-on-string structures. The exponential decay regime observed during the filament thinning process is used to calculate the steady extensional viscosity of all DNA suspensions. Results show that semi-dilute T4 DNA suspensions are extensional strain rate thinning, while dilute DNA suspensions are nearly Newtonian. Single molecule visualization of λ-DNA shows that individual molecules transition from a coiled state to an almost fully stretched state when experiencing extensional flow within the filament. However, the DNA stretch dynamics are heterogeneous due to molecular individualism and initial conditions.

2. Experimental methods

The experimental configuration is a cross-slot microchannel that is $W = 100$ μm wide and $L = 100$ μm deep, shown in Fig. 1. The device is molded in polydimethylsiloxane (PDMS) using standard lithography methods.[46,47] Channels are sealed with a glass cover slip after exposure to an oxygen plasma for 15 s. The assembled channels are then baked for approximately 12 h at 65 °C to obtain hydrophobic walls wetted by the continuous oil phase.

The outer continuous phase is mineral oil containing 0.1% by weight surfactant (SPAN 80). Both the Newtonian fluid and DNA suspensions are used as the inner aqueous phase. The Newtonian fluid is a solution of 91%-glycerin by weight and Tris-EDTA (TE) buffer. The DNA suspensions are made by adding DNA molecules to a Newtonian viscous solvent. A viscous solvent is used to (i) match the shear-viscosity of the oil so that the viscosity ratio is close to one, and (ii) increase the hydrodynamic stresses around the molecule in order to enhance any elastic effects that may occur. The interfacial tension σ between the continuous mineral oil and all aqueous phases is approximately 0.01 N m^{-1}. The level of fluid elasticity is varied by (i) selecting DNA molecules of different molecular weights (MWs) and (ii) adjusting the DNA concentration in the Newtonian solvent.

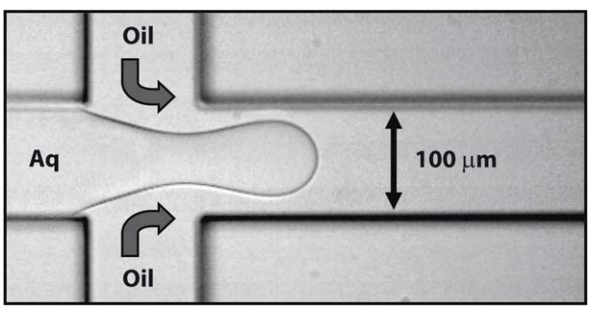

Fig. 1 The experimental setup illustrating drop formation at the center of the cross-slot microchannel. The device is molded in PDMS and channel dimensions are 100 μm wide and 100 μm deep. The oil phase and the aqueous phase (Newtonian fluid and DNA suspensions) are injected into the device using low noise syringe pumps at inlets located 1 centimetre from the center of the cross-slot.

The molecular weight of the double-stranded DNA molecules is varied by using two molecules of different sizes, namely λ-phage DNA and T4 DNA. The λ-phage DNA molecules have 48.5 × 10^3 base-pairs while T4 DNA molecules have 165.6 × 10^3 base-pairs. The MWs of λ-DNA and T4 DNA are 3 × 10^7 g mol^{-1} and 1 × 10^8 g mol^{-1}, respectively. For both molecules, the distance between base-pairs is approximately 0.34 nm. Therefore, in buffer solution and at room temperature, the molecular contour lengths are approximately 16.5 μm for λ-DNA and 56.3 μm for T4 DNA. The DNA molecules are dispersed in a TE buffer-glycerin mixture at normalized concentrations of either $c/c^* \approx 0.5$ or $c/c^* \approx 1$, where c^* is the overlap concentration. The values of c^* for λ-DNA and T4 DNA are approximately 40 μg mL^{-1} and 19 μg mL^{-1}, respectively. Note that $c^* \propto R_g^{-3}$, where R_g is the molecule's radius of gyration.[49,50] The properties of both molecules are summarized in Table 1.

All fluids are characterized using a stress-controlled rheometer (Fig. 2). The shear viscosities of the oil and Newtonian fluids are nearly identical and independent of shear rate: $\mu = 0.25 \pm 0.02$ Pa s. At low shear-rates, the viscosities of the DNA solutions show slight shear thinning behavior with an average power law index of 0.80. Beyond a shear-rate of 1 s^{-1}, the DNA suspensions are nearly Newtonian with viscosity values of approximately 0.25 Pa s. No appreciable first normal stress differences were detected.

The aqueous and continuous oil phases are injected into the central and side arms of the cross channel, respectively, using low-noise syringe pumps. Experiments are performed for flow rate ratios, $q = Q_{oil}/Q_{aq}$, of 10, 20, and 30. In all cases, the aqueous flow rate is kept constant at $Q_{aq} = 0.02$ μL min^{-1}. This value of Q_{aq} is chosen so that the behavior is quasi-static, such that the periodicity, but not the morphology, depends on Q_{aq}. For this range of parameters, the Reynolds number Re defined as $\rho VL/\mu$ is less than 0.01, the capillary number Ca defined as $\mu V/\sigma$ ranges from 0.008 to 0.02, and the Ohnesorge number Oh defined as $\mu/\rho\sigma L$ is approximately 10; therefore viscous forces are much larger than both inertial and surface forces. Here, L and V

Table 1 Properties of λ-DNA and T4 DNA molecules are presented. Here, L is the theoretical contour length of fluorescently stained DNA with YOYO-1 dye, R_g is the molecule radius of gyration, and c^* is the critical overlap concentration.[18,48]

molecule	base-pair (kbp)	MW (g mol^{-1})	L (μm)	R_g (μm)	c^*(μg mL^{-1})
λ-DNA	48.5	3 × 10^7	22	0.73	40
T4 DNA	165.6	1 × 10^8	67	1.64	19.2

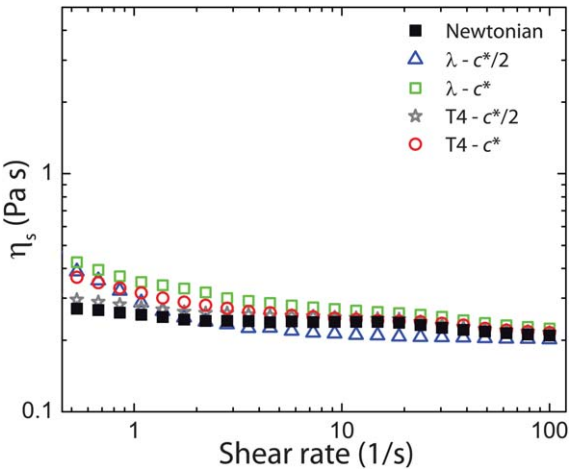

Fig. 2 (Color online) Fluid rheological characterization. Shear viscosity *versus* shear strain rate for the Newtonian fluid and all DNA suspensions. DNA suspensions display slight shear thinning behavior with an average power law index of 0.80. The values of shear viscosities are nearly constant at a value of approximately 0.25 Pa s for all fluids beyond 1 s^{-1}.

are the characteristic fluid length and velocity, ρ and μ are the fluid density and viscosity, and σ is the surface tension. Under these conditions an aqueous filament is formed and stretched by the flow of the surrounding oil. The thinning and breakup of the filament are imaged using an inverted microscope at 63× magnification and a fast video camera with frame rates between 1 and 10 kHz.

3. Results

Fig. 3, and the ESI,† show sample snapshots of the evolution of the filament thinning and drop breakup processes as a function of normalized time t/t_b, where t_b is the breakup time, for a Newtonian fluid (left), λ-DNA suspension (center), and T4 DNA suspension (right). The normalized concentration c/c^* of the DNA suspensions is approximately 1, and the flow rate ratio $q = Q_{oil}/Q_{aq}$ is 30. The time zero ($t = 0$) is computed when the negative curvature of the filament interface first occurs in the mother drop, and the breakup time (t_b) is determined when the filament becomes discontinuous (Fig. 3). For the Newtonian fluid ($t_b = 85$ ms), the aqueous filament is initially drawn into the cross-slot and then stretched by the surrounding oil flow ($t/t_b = 0.15$). The filament is further elongated by the continuous phase ($t/t_b = 0.45$), and begins to thin quite rapidly ($t/t_b = 0.95$). Finally, the filament reaches the pinch-off point where it breaks into a large primary drop and small satellite drops ($t > t_b$).

The snapshots of the semi-dilute λ-DNA (MW 10^7) suspension show that at early times ($t/t_b < 0.45$) the filament thinning process is very similar to that of the Newtonian case. At later times ($t/t_b > 0.45$), however, the fluid filaments exhibit different features. In particular, the presence of DNA molecules in the fluid leads to relatively long fluid threads and a delay in breakup time ($t_b = 120$ ms) compared to the Newtonian case. Near the pinch-off event ($t/t_b = 0.95$), the filament contains multiple drops attached by a thin fluid thread, a morphology that is commonly referred to as beads-on-a-string.[51,52]

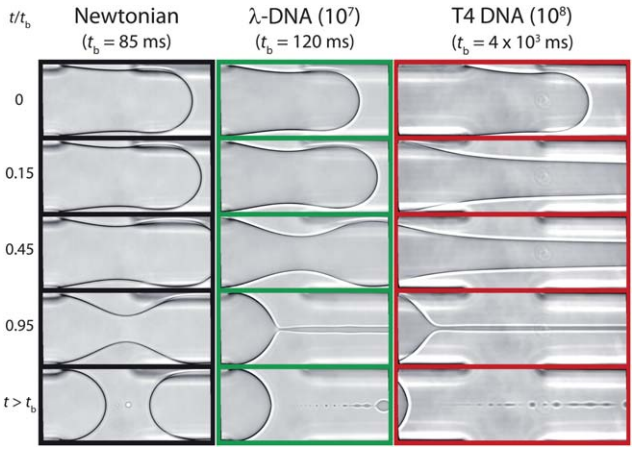

Fig. 3 (Color online) Evolution of the thinning process for the Newtonian fluid (left column) and DNA suspensions with a normalized concentration of $c/c^* \approx 1$ and MWs equal to 10^7 (middle column) and 10^8 (right column) for a flow rate ratio of $q = Q_{oil}/Q_{aq} = 30$. Time progresses from top to bottom and the breakup times t_b of the Newtonian fluid, λ-DNA, and T4 DNA suspensions for this flow rate ratio are 85, 120, and 4×10^3 ms, respectively. The images are taken at 63× magnification and located at the center of the cross-slot with flow occurring from left to right. The window for the Newtonian and λ-DNA cases represents 236 × 100 μm² while the window for T4 DNA case is 321 × 100 μm². See the ESI.†

The filament thinning and drop breakup processes of the semi-dilute T4 DNA (MW 10^8) suspension are very different from the Newtonian fluid and λ-DNA suspension. The snapshots show that the presence of larger DNA molecules in the fluid results in the development of a very long filament ($t/t_b = 0.45$) and delayed breakup time ($t_b = 4 \times 10^3$ ms). Near pinch-off ($t/t_b = 0.95$), the primary drop is still attached to the mother drop by the long thin fluid thread, which shows periodic beads along the filament. After breakup, there are many satellite drops. These observations are qualitatively similar to the thinning and breakup of viscoelastic fluid threads in microchannels[45,53] and in macroscopic drop breakup experiments.[32,40] The extra elastic stresses are provided, in this case, by the DNA molecules in the fluid.

Effects of DNA molecules in fluid filaments

The filament thinning process is quantified by the decrease in filament diameter h as a function of time. To accomplish this, we determine the interface contour between the aqueous and surrounding oil phases within the cross-slot region. It was previously shown that the exact measurement location has little impact on the overall filament thickness data,[45] and we only present measurements of the minimum filament thickness in the field of view (Fig. 4). Multiple filament thinning and drop breakup events are recorded for each fluid at each flow ratio.

Results of a representative trial are shown in Fig. 4 for the Newtonian fluid and the DNA suspensions for three flow rate ratios, $q = 10$, 20, and 30. At short times, approximately $t < 20$ ms, the Newtonian fluid and all DNA suspensions exhibit identical thinning behavior due to their similar values of shear viscosity μ (Fig. 2). For the Newtonian case, it has been shown that the filament thins with a single exponential regime until near the

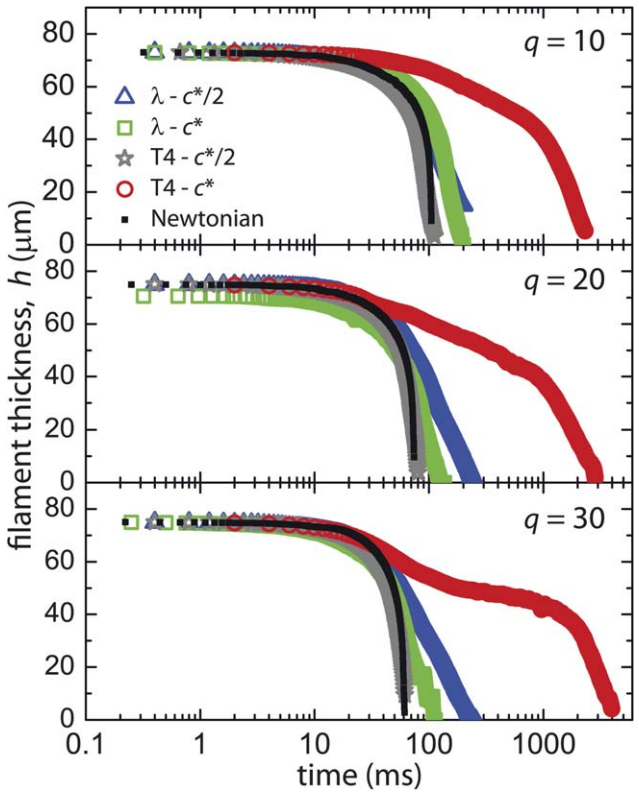

Fig. 4 (Color online) Minimum filament thickness h as a function of time for the Newtonian fluid and all DNA suspensions at three different flow rate ratios $q = Q_{oil}/Q_{aq}$, where $Q_{aq} = 0.02$ μL min^{-1}. Initially, for all fluids and q, the values of h are nearly identical since all fluids have similar values of shear-viscosity. The Newtonian fluid and the dilute DNA suspensions undergo a single exponential thinning regime ($t < 20$ ms). Similar behavior is observed fro the semi-dilute low MW (10^7) λ-DNA suspension. The high MW (10^8) semi-dilute T4 DNA suspension undergoes a second exponential thinning at later times.

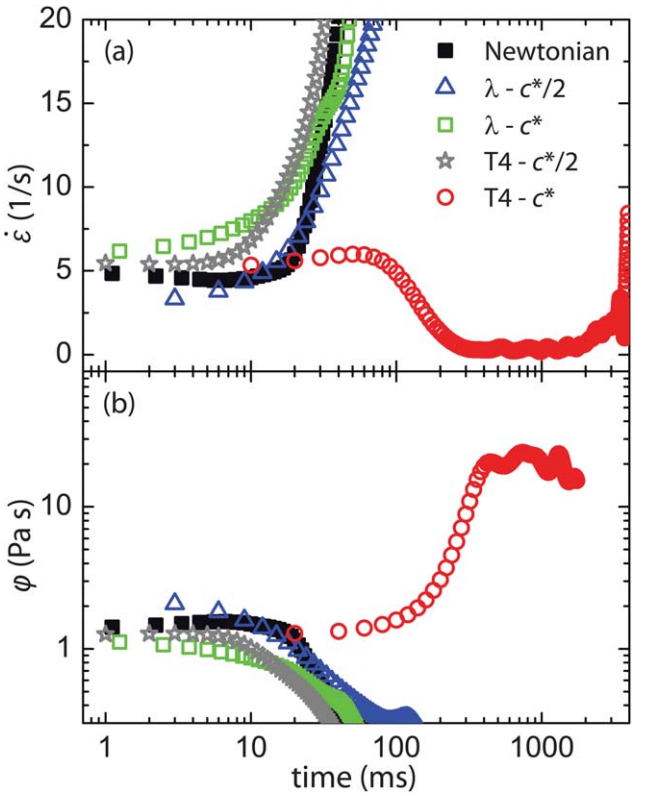

Fig. 5 (Color online) Time dependent filament extensional strain rate $\dot{\varepsilon}$ and the quantity φ for the Newtonian fluid and the DNA suspensions for the flow ratio $q = 30$. (a) The exponential thinning regimes are characterized by constant values of $\dot{\varepsilon}$, seen to occur during the first $t < 15$ ms. (b) The quantity φ is equivalent to the filament steady extensional viscosity η_e when $\dot{\varepsilon}$ is constant. Initially, for all fluids, the values of φ are similar since all fluids have nearly the same shear viscosity μ. At later times (300 ms to 2×10^3 ms), however, φ increases significantly for semi-dilute T4 DNA suspensions.

filament breakup (*cf.* Fig. 5).[45,53] At later times, near the breakup point, the presence of DNA molecules in the fluid can affect the thinning process. For the dilute DNA suspensions, the filaments thin with a single exponential regime but at a slower rate than the Newtonian case even though all fluids have the same shear viscosity.

In the semi-dilute regime, we find that the MW has a significant impact on the fluid thinning process. While the semi-dilute λ-DNA (MW 10^7) suspensions show similar behavior than the dilute suspensions, the semi-dilute T4 DNA (MW 10^8) suspension displays a second exponential decay typical of viscoelastic fluids.[45,54] This result indicates that the elastic stresses due to the presence of DNA molecules in the fluid has a stabilizing effect on the filament. Moreover, this strongly suggests that the thinning process is governed by a balance between the outer fluid viscous stress and the inner fluid viscoelastic stress, which is an important assertion for later calculations of the extensional viscosity.

We further quantify these observations by computing the filament strain rate from the measured values of filament thickness. Here, the filament extensional strain rate is defined as $\dot{\varepsilon} = -(2/h)\mathrm{d}h/\mathrm{d}t$.[32,40] In Fig. 5 (a), the values of strain rate $\dot{\varepsilon}$ are shown as a function of time for the Newtonian fluid and the DNA suspensions at the flow rate ratio $q = 30$. Initially for $t < 20$ ms, the Newtonian fluid has a nearly constant value of $\dot{\varepsilon}$, which corresponds to the single exponential thinning regime (Fig. 4). The dilute DNA suspensions have similar values of $\dot{\varepsilon}$ to that of the Newtonian case and are also independent of time.

For the semi-dilute regime, the MW affects the extensional strain rate at later times during the thinning process. The lower MW, semi-dilute λ-DNA suspension (MW 10^7) shows similar behavior than the dilute suspensions and the Newtonian case. The higher MW, semi-dilute T4 DNA suspension (MW 10^8) is unique in that a second exponential thinning regime is observed in which $\dot{\varepsilon}$ is constant. For this case, the values of $\dot{\varepsilon}$ are initially constant and equal in magnitude to the Newtonian and dilute DNA cases. However, after a transient interval, $\dot{\varepsilon}$ reaches a smaller (and constant) value than the other suspensions. This second exponential thinning regime occurs from $t = 300$ ms to $t = 2 \times 10^3$ ms (Fig. 5a). Overall, the exponential thinning of the fluid threads in all fluids investigated here indicates that the flow inside the fluid thread is extensional. Hence, it is possible to calculate the steady extensional viscosity of the Newtonian fluid and DNA suspensions in these exponential thinning regimes.

We note that, for all fluids, at the very latest times close to breakup, the final decrease of h to zero gives an apparent divergence of $\dot{\varepsilon}$. It was previously shown that just before breakup,[45] the data are consistent with a linear decrease in filament diameter, such that $h(t) \propto (t - t_b)$.

Simple model for filament thinning

We model the exponential decay in filament thickness by assuming that (i) filament thinning is driven mainly by the outer fluid (oil) extensional flow in the cross-slot region and (ii) the shear flow that develops is relatively far downstream from the cross-slot region and should have no implications for the local stress balance. These are reasonable assumptions since shear stresses tangential to the filament do not contribute to the thinning (or squeezing) of the filament. In the cross-slot region, the filament thinning is driven by viscous stresses normal to the filament.

The exponential thinning is driven by the outer fluid (oil) flow. In this flow-driven regime, the stress balance inside and outside the interface is $\eta_e\dot{\varepsilon} = \eta_{e,oil}\dot{\varepsilon}_{oil}$. This balance relates the extensional strain rates and extensional viscosities of the aqueous (Newtonian fluid and DNA suspensions) and oil phases. Since the oil is a Newtonian fluid, we apply the definition of extensional viscosity so that $\eta_{e,oil} = 3\mu_{oil}$. As mentioned before, the fluid filament strain rate is defined as $\dot{\varepsilon} = -(2/h)\mathrm{d}h/\mathrm{d}t$. The strain rate for oil in the cross-slot region is $\dot{\varepsilon}_{oil} \approx Q_{oil}/(W^2L)$, as verified by particle tracking methods.[55] Here, W is the channel width and L is the channel depth. Assuming that η_e is independent of time, then the filament diameter thins according to

$$h(t) = h_0\exp[-(3/2)(\mu_{oil}/\eta_e)\dot{\varepsilon}_{oil}t], \quad (1)$$

where h_0 is an integration constant. This equation is only valid for the flow-driven exponential regimes shown in Fig. 4. In such flow-driven regimes, eqn (1) may be used to deduce the values of η_e from $h(t)$ data in regions where the filament extensional strain rate $\dot{\varepsilon}$ is constant (Fig. 5a).

Steady extensional viscosity of DNA suspensions

In order to illustrate how the *steady* extensional viscosity of all fluids is calculated, the quantity φ, defined as $\varphi = \eta_{e,oil}\dot{\varepsilon}_{oil}/\dot{\varepsilon}$, is plotted as a function of time (Fig. 5b). Note that φ has units of viscosity, and regions in which both this quantity and the strain rate are constant correspond to extensional viscosity values for that particular strain rate. For example, the Newtonian fluid shows an approximately constant value of $\varphi = 1.41$ Pa s for $q = 30$ for the first $t < 20$ ms. The temporal average of all φ values during this time interval correspond to $\eta_e = 1.41$ Pa s at $\dot{\varepsilon} = 4.91\ s^{-1}$. For the semi-dilute T4 DNA suspensions, however, the second exponential regime at the highest flow ratio q is used to calculate η_e.

Fig. 6 shows values of the steady extensional viscosity η_e for all aqueous solutions as a function of the filament extensional strain rate $\dot{\varepsilon}$. The average value of η_e for the Newtonian fluid is approximately 0.85 Pa s, which is close to $3\bar{\mu} = 0.75$ Pa s. The values of η_e for the Newtonian fluid are independent of extensional strain rate, as expected. The dilute DNA suspensions show values of η_e that are slightly larger than the Newtonian and also

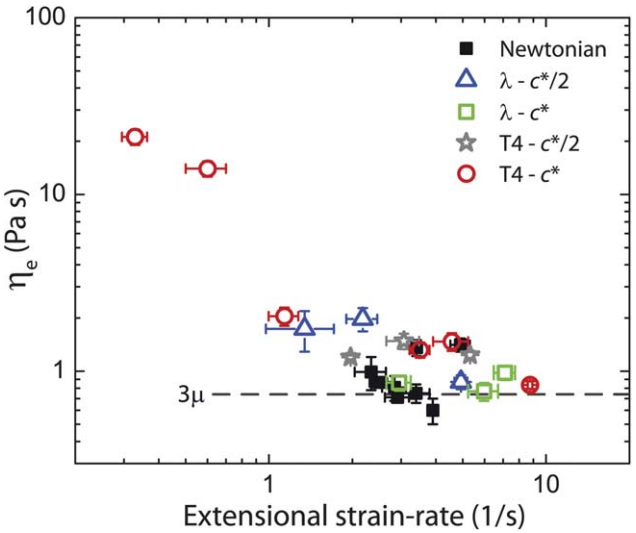

Fig. 6 (Color online) Steady extensional viscosity η_e, obtained from the flow-drive regime described by eqn (1), *versus* the extensional strain rate $\dot{\varepsilon}$ for the Newtonian fluid and all DNA suspensions. The values of η_e for the Newtonian fluid are independent of strain rate and are in close agreement with $\eta_e = 3\bar{\mu}$, represented by the dashed line. The dilute DNA suspensions values of η_e that are slightly larger than $3\bar{\mu}$, but are independent of strain rate. Similar behavior is observed for the low MW (10^7) semi-dilute λ-DNA suspension. The values of the steady extensional viscosity for the high MW (10^8) semi-dilute T4 DNA suspension exhibits strain rate thinning behavior over the values of $\dot{\varepsilon}$ examined.

appear to be independent of $\dot{\varepsilon}$ for the extensional strain rates examined here. The same behavior is observed for the semi-dilute λ-DNA (MW 10^7) suspension. However, over the range of extensional strain rates examined, the semi-dilute T4 DNA (MW 10^8) suspension exhibits extensional strain rate thinning behavior. This behavior is similar to other complex fluids[30] such as wormlike micelle solutions[56] and carbon nanofiber suspensions.[57] Possible mechanisms that could explain the thinning extensional viscosity behavior include molecular scission degradation[58,59] and polymer rigidity.[60]

4. DNA stretch dynamics in fluid filaments

One advantage of this microfluidic extensional rheometer is that it allows for simultaneous visualization of the bulk fluid behavior as well as the individual DNA molecules within the fluid. To gain further insight into the filament thinning process of aqueous solutions, we performed identical experiments as described above but with fluorescently labeled λ-DNA. It is known that for long, flexible polymer chains such as DNA, the preferred entropic state is that of a coiled conformation that is often described by the radius of gyration R_g. When polymer molecules are in regions of high velocity gradients, they are stretched and aligned with the direction of the flow.[3] It is believed that the change in conformation of the molecules, from coiled to stretched, is in part responsible for the enhanced extensional viscosity of complex fluids compared to simple, Newtonian liquids.[34]

Semi-dilute λ-DNA suspensions, similar to those described in the experimental methods section, are used here with slight modification. Briefly, λ-DNA stock solution is heated at 65 °C for

10 min and then quenched in an ice bath. A percentage of the λ-DNA molecules (15% v/v) are stained with YOYO-1 iodide, a bis-intercalating dye, at a dye to base pair ratio of 1 : 4. The solution is allowed to incubate at room temperature for at least 1 h. Stained and unstained λ-DNA are then added to a viscous Newtonian solvent that is 91% (w/w) glycerin and 4% (v/v) β-mercaptoethanol, which is added to reduce photo-bleaching. The final concentration of λ-DNA molecules in the buffer-glycerin solution is $c/c^* \approx 1$. The DNA molecules are visualized using high-speed epifluorescence microscopy that consisted of a 100×, 1.4 NA oil immersion objective and an image-intensified CMOS camera. Fluorescence illumination is supplied by a 100 W mercury lamp. Image acquisition ranged from 250 to 1000 Hz.

High speed image acquisition is required in order to visualize molecules during the entire thinning process. Example snapshots of fluorescently labeled DNA molecules in a semi-dilute λ-DNA suspension undergoing filament thinning are shown in Fig. 7 for $q = 10$. The area of fluorescence illumination is circular with a radius of 50 μm. The interface between the oil and aqueous phases is represented by the white line. Fig. 7 (a) shows that, before the filament thinning process begins, the DNA molecules are mostly in their coiled (equilibrium) state. Some pre-shearing, however, is evident by noting (qualitatively) that a small number of molecules are somewhat stretched. At a later time (Fig. 7b), molecules are elongated far from their equilibrium state, although the distribution is not uniform. After breakup of the fluid filament, molecules return to a coiled state as the surrounding fluid elements relax (not shown here). We found no evidence of molecular scission in our experiments.

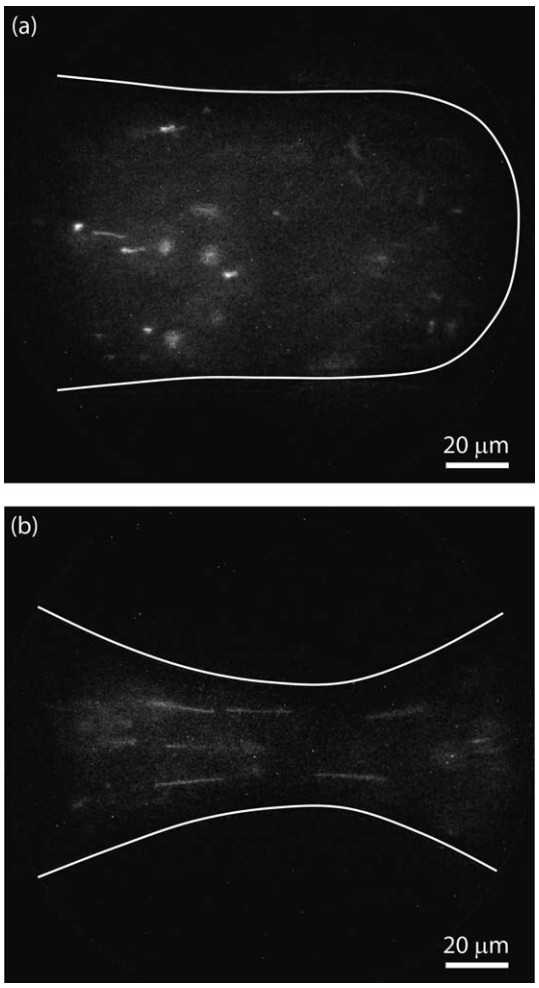

Fig. 7 Visualization of fluorescent λ-DNA molecules in thinning fluid filaments for $q = 10$. Frame rate acquisition is 250 Hz. The white line represents the interface between the oil phase and the semi-dilute DNA suspension. (a) Initially, during the formation of the mother drop at $t = 0$, the majority of λ-DNA molecules are in a coiled equilibrium state, with few exceptions due to pre-shear. (b) At later times $t/t_b = 0.5$, λ-DNA molecules become fully stretched and aligned due to the strong flow inside filaments.

We quantify the stretching dynamics of DNA molecules in thinning fluid filaments by measuring the molecule's total length x, or major axis, at five different instances during the drop breakup process, $t = 0$, $t/t_b = 0.1$, $t/t_b = 0.2$, $t/t_b = 0.3$, $t/t_b = 0.4$, and $t/t_b = 0.5$. The values of x are normalized by the theoretical maximum contour length, $L_0 = 22$ μm, of stained λ-DNA.[18,48] Multiple drop breakup events are recorded in order to sample a large number of stretching events at different locations within the filaments. Only those molecules that remained in focus are included in the analysis. For these reasons, measurements for $t/t_b > 0.5$ are not discussed here due to the sparse observations of fluorescent DNA within the filament.

Fig. 8 shows the probability distribution functions (PDFs) of the normalized stretch length x/L_0 of fluorescent λ-DNA molecules in solution at the initial stage of drop formation $t = 0$ and at later times in the breakup process, $t/t_b = 0.3$ and $t/t_b = 0.5$. The distribution of x/L_0 values at $t = 0$ is narrow and peaked around a value of 0.2 (Fig. 8a). This distribution corresponds to molecules that are mostly coiled, with the majority of the normalized extensions ranging from 0.1 to 0.4. There are few exceptions with a small percentage of molecules with normalized extensions of up to 0.5. The first moment of this PDF is $x/L_0 = 0.22$, or $x = 4.8$ μm, which is largely due to pre-shearing as molecules travel through the microfluidic device.

As the thinning process continues $t/t_b = 0.3$, the distribution of normalized stretch lengths begins to broaden with stretch values ranging from $0.1 < x/L_0 < 0.8$. The strong flow inside the thinning filament causes molecules that were originally coiled at equilibrium to transition to a partially stretched state (Fig. 8b). At even later times $t/t_b = 0.5$, values of the normalized extension vary over the entire range $0.1 < x/L_0 < 1.0$, with double peaks around values of $x/L_0 = 0.4$ and $x/L_0 = 1.0$ (Fig. 8c). This broad PDF corresponds to a heterogeneous distribution of molecular contour lengths, from partially stretched to fully elongated (Fig. 7b). The broad distributions observed here can be the result of many factors including conformational and spatial initial conditions. Depending on the initial position of the molecule within the fluid filament, the molecule will experience different velocity gradients (and hydrodynamic drag), which will result in different overall stretch length. For example, molecules near the center of the filament are linearly stretched to near full length and aligned with the outflow along the filament axis. Molecules farther from the center of the filament are only partially stretched, but still aligned along the filament axis.

Another possible mechanism for a broad distribution in stretch length is due to molecular individualism[5] of DNA. In the coiled state, molecules are constantly changing shape due to Brownian motion and can adopt any number of configurations.

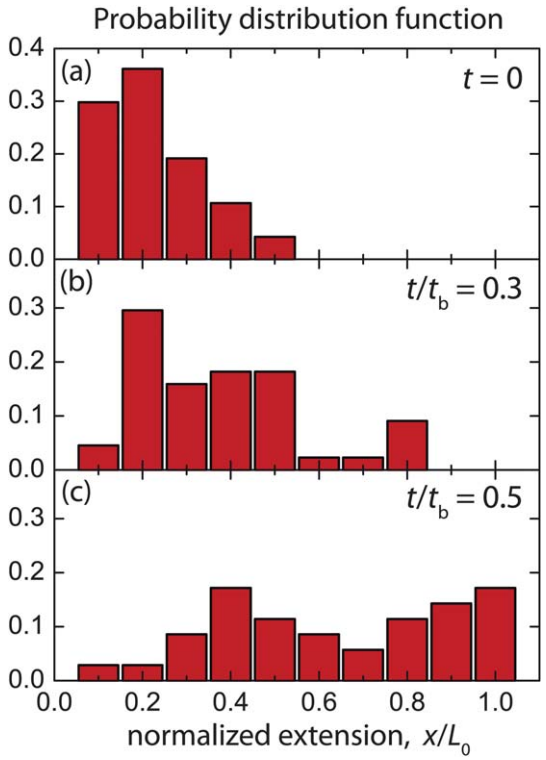

Fig. 8 Probability distribution functions of the normalized extension x/L_0 of λ-DNA molecules in fluid filaments. (a) Initially at $t = 0$, the majority of molecules are in a relaxed coiled state, producing a narrow PDF peaked around a value of $x/L_0 = 0.2$. (b) At a later time ($t/t_b = 0.3$), the distribution begins to broaden as molecules transition from a coiled state to a partially elongated state due to the increase in surrounding velocity gradients. (c) At even later times ($t/t_b = 0.5$), the PDF broadens further and we observe a range of normalized stretch values from $0.1 < x/L_0 < 1.0$, which corresponds to molecules that are only partially stretched to fully elongated.

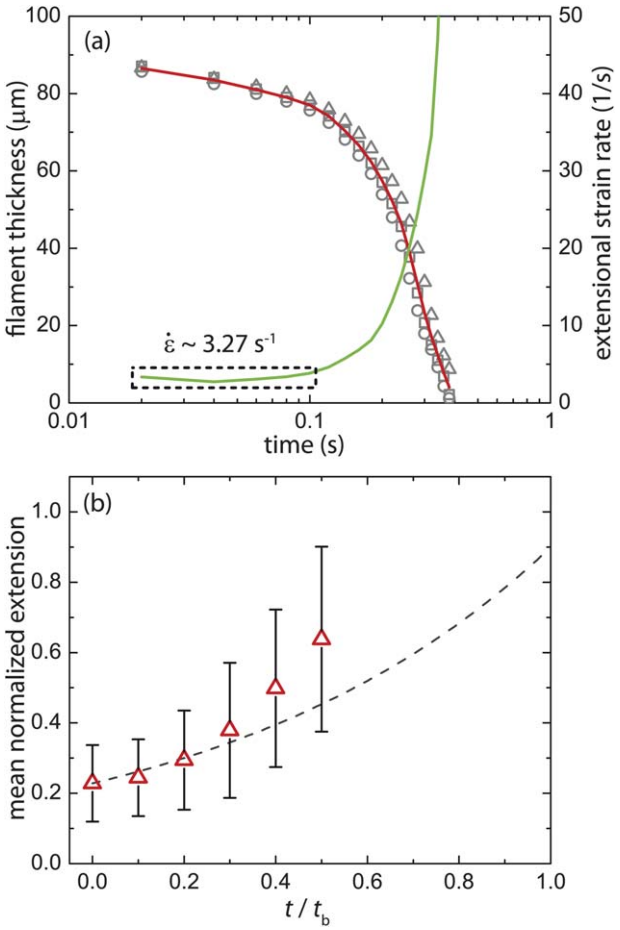

Fig. 9 (Color online) (a) The fluid filament diameter and the corresponding extensional strain rate as a function of time for semi-dilute λ-DNA suspensions for flow ratio $q = 10$. Data points represent individual filament thinning measurements while the solid curves represent the average of all measurements. The extensional strain rate is constant at 3.27 s^{-1} over the first 70 ms during the flow-driven regime. (b) The mean normalized stretch length of fluorescent λ-DNA molecules in thinning fluid filaments as a function of normalized time. The average values are obtained from the first moment of the PDFs and errors bars represent the standard deviation. The mean normalized stretch length and the standard deviation about the mean increase due to the heterogeneous distribution of molecule stretch lengths. The dashed curve represents the deformation of a fluid element under uniform extensional flow.

As the filament begins to thin and the hydrodynamic stresses around the molecule increase, differences in initial conformation can lead to different stretch dynamics. For example, it has been shown that, in planar elongational flows,[5] molecules exposed to the same velocity gradients may evolve to different conformation shapes such as kinked, folded, or dumb-bell due to slight differences in initial conformation. In the experiments presented here, two different molecules with similar initial positions in the fluid filament are not expected to reach similar stretch lengths due to differences in initial conformation. Therefore, the distribution of molecular stretch lengths within the fluid filament becomes heterogeneous.

The simultaneous visualization of individual DNA molecules and of the bulk flow behavior enables the direct connection between the bulk fluid measurements and molecule conformation dynamics. Fig. 9(a) shows representative measurements of the filament diameter h and the extensional strain rate $\dot{\varepsilon}$ as a function of time for fluorescently labeled λ-DNA suspensions for $q = 10$ and $c/c^* = 1$. Fig. 9(b) shows the mean normalized extension $\bar{x}/L_0$ of single molecules (same fluid as 9a) as a function of normalized time t/t_b, where t_b is the breakup time. We observe that both the $\bar{x}/L_0$ values and its standard deviation increase with time, as discussed before (Fig. 8).

In order to gain further insight into the stretching dynamics of DNA molecules inside a thinning fluid thread, we compare the results in Fig. 9(b) with the deformation of a fluid element in an uniform extensional flow that evolves according to $L(t) = L_0\exp(\dot{\varepsilon}_0 t)$. The initial size L_0 of the fluid element is 0.22, which corresponds to the initial mean molecular stretch value, and the strain rate is $\dot{\varepsilon} = 3.27\ s^{-1}$, which corresponds to the fluid filament thinning rate in Fig. 9(a). We find that this uniform extension curve is in good agreement with the molecular data up to $t/t_b = 0.4$ only, where the strain rate is actually constant. The agreement between the average stretch lengths with the stretching of a fluid element in extensional flows suggests the possibility of using DNA molecules as elastic stress sensors in complex time dependent flow structures common to non-Newtonian fluids.[61]

5. Conclusions

An experimental investigation on the dynamics of filament thinning and drop breakup of DNA suspensions in a cross-slot microchannel is presented. This microfluidic device allows for the simultaneous visualization of individual DNA molecules and of the bulk flow behavior. We find that Newtonian fluids and the dilute DNA suspensions undergo a single exponential thinning regime. The dilute DNA suspensions, however, display a slower exponential decay rate than the Newtonian case. The semi-dilute λ-DNA (MW 10^7) suspensions show similar behavior than the dilute suspensions, but the semi-dilute T4 DNA (MW 10^8) suspension displays a second exponential decay typical of viscoelastic fluids.[45,54] This elastic behavior is most likely due to the stretching of the large DNA molecules inside the fluid filament undergoing breakup. The measured extensional viscosity of this semi-dilute T4 DNA suspension shows an extensional strain rate thinning behavior. This thinning behavior is also observed in other semi-flexible fluids such micellar solutions and suspensions of carbon-nanofibers.

Direct visualization of fluorescently labeled DNA molecules in a semi-dilute λ-DNA suspension undergoing filament thinning are also performed. This is the first time such molecular observations are made inside a fluid filament undergoing thinning and breakup. Many drop breakup events are recorded in order to obtain better insights into the stretching dynamics of single molecules within thinning fluid filaments. The probability distribution functions (PDFs) of the normalized stretch length (x/L_0) of fluorescent DNA molecules are used to quantify the dynamics. At the beginning of the breakup process, the majority of molecules are in an equilibrium coiled conformation that is described by a narrow PDF peaked around $x/L_0 = 0.2$. As the thinning process progresses, molecules transition from coiled to a partially elongated state due to the strong flow inside the thinning filament, which produces a broader PDF. At later times, most of the fluorescent λ-DNA molecules are observed to reach full extension. The broad stretch distribution at later times is most likely due to "molecular individualism" and initial conditions. Despite the broad distributions, the average stretch length as a function in time agrees well with affine fluid stretching for short times only.

Filament thinning of DNA fluids provides an efficient method for stretching individual DNA molecules, as well as other semi-flexible polymers, through hydrodynamic stress alone. The strong flows created by thinning filaments can align and stretch molecules to full theoretical extension in the absence of an external probe,[62,63] electric field,[64] temperature gradients,[65] or by confinement effects of nanochannels.[66] This method of stretching and aligning DNA molecules in two-phase flows may find application in genomic studies, polymerase chain reaction (PCR), and molecular coding among others.

Acknowledgements

We thank X. N. Shen for assistance regarding fluid characterization and rheology, C. Wagner for assistance regarding single molecule high speed imaging and optics, and Y. Ren and D. Stein for helpful discussions regarding fluorescent DNA preparation and image analysis. This work was supported by the National Science Foundation through the award CBET-0932449.

References

1 N. Wang, *Hypertension*, 1998, **32**, 162–165.
2 V. A. Bloomfield, *Biopolymers*, 1997, **44**, 269–282.
3 P. G. de Gennes, *J. Chem. Phys.*, 1974, **60**, 5030–5042.
4 A. Keller and J. A. Odell, *Colloid Polym. Sci.*, 1985, **263**, 181–201.
5 T. T. Perkins, D. E. Smith and S. Chu, *Science*, 1997, **276**, 2016–2021.
6 C. M. Schroeder, E. S. G. Shaqfeh and S. Chu, *Macromolecules*, 2004, **37**, 9242–9256.
7 E. S. G. Shaqfeh, *J. Non-Newtonian Fluid Mech.*, 2005, **130**, 1–28.
8 E. Y. Chan, *et al.*, *Genome Res.*, 2004, **14**, 1137–1146.
9 R. Riehn, *et al.*, *Proc. Natl. Acad. Sci. U. S. A.*, 2005, **102**, 10012–10016.
10 R. Dylla-Spears, *et al.*, *Lab Chip*, 2010, **10**, 1543–1549.
11 J. S. Bader, *et al.*, *Proc. Natl. Acad. Sci. U. S. A.*, 1999, **96**, 13165–13169.
12 R. Ashton, C. Padala and R. S. Kane, *Curr. Opin. Biotechnol.*, 2003, **14**, 497–504.
13 E. D. T. Aktins and M. A. Taylor, *Biopolymers*, 1992, **32**, 911–923.
14 T. T. Perkins, D. E. Smith and S. Chu, *Science*, 1994, **264**, 819–822.
15 J. O. Tegenfeldt, *et al.*, *Proc. Natl. Acad. Sci. U. S. A.*, 2004, **101**, 10979–10983.
16 D. Stein, F. H. van der Heyden, W. Koopmans and C. Dekker, *Proc. Natl. Acad. Sci. U. S. A.*, 2006, **103**, 15853–15858.
17 S. Gerashchenko and V. Steinberg, *Phys. Rev. Lett.*, 2006, **96**, 038304.
18 C. C. Hsieh and P. S. Doyle, *Korea-Aust. Rheol. J.*, 2008, **20**, 127–142.
19 D. J. Bonthuis, C. Meyer, D. Stein and C. Dekker, *Phys. Rev. Lett.*, 2008, **101**, 108303.
20 S. Gulati, S. J. Muller and D. Liepmann, *J. Non-Newtonian Fluid Mech.*, 2008, **155**, 51–66.
21 O. L. Hemminger, P. E. Boukany, S. Q. Wang and L. J. Lee, *J. Non-Newtonian Fluid Mech.*, 2010, **165**, 1613–1624.
22 D. E. Smith and S. Chu, *Science*, 1998, **281**, 1335–1340.
23 D. Smith, H. Babcock and S. Chu, *Science*, 1999, **283**, 1724–1727.
24 H. P. Babcock, *et al.*, *Macromolecules*, 2003, **36**, 4544–4548.
25 R. Duggal and M. Pasquali, *J. Rheol.*, 2004, **48**, 745–764.
26 S. Gerashchenko, C. Chevallard and V. Steinberg, *Europhys. Lett.*, 2005, **71**, 221–227.
27 T. G. Mason, A. Dhople and D. Wirtz, *Macromolecules*, 1998, **31**, 3600–3603.
28 D. Jary, J.-L. Sikorav and D. Lairez, *Europhys. Lett.*, 1999, **46**, 251–255.
29 J. S. Hur, E. S. G. Shaqfeh, H. P. B. D. E. Smith and S. Chu, *J. Rheol.*, 2001, **42**, 421–450.
30 R. K. Gupta, D. A. Nguyen and T. Sridhar, *Phys. Fluids*, 2000, **12**, 1296–1318.
31 S. L. Anna, *et al.*, *J. Rheol.*, 2001, **45**, 83–114.
32 S. L. Anna and G. H. McKinley, *J. Rheol.*, 2001, **45**, 115–138.
33 R. Sattler, C. Wanger and J. Eggers, *Phys. Rev. Lett.*, 2008, **100**, 164502.
34 G. McKinley and T. Sridhar, *Annu. Rev. Fluid Mech.*, 2002, **34**, 375–415.
35 M. S. N. Oliveira, R. Yeh and G. H. McKinley, *J. Non-Newtonian Fluid Mech.*, 2006, **137**, 137–148.
36 A. Bhardwaj, E. Miller and J. P. Rothstein, *J. Rheol.*, 2007, **51**, 693–719.
37 C. Clasen, *Korea-Aust. Rheol. J.*, 2010, **22**, 331–338.
38 H.-C. Chang, E. A. Demekhin and E. Kalaidin, *Phys. Fluids*, 1999, **11**, 1717–1737.
39 Y. Christanti and L. M. Walker, *J. Non-Newtonian Fluid Mech.*, 2001, **100**, 9–26.
40 Y. Amarouchene, D. Bonn, J. Meunier and H. Kellay, *Phys. Rev. Lett.*, 2001, **86**, 3558–3561.
41 C. Wagner, Y. Amarouchene, P. Doyle and D. Bonn, *Europhys. Lett.*, 2003, **64**, 823–829.
42 V. Tirtaatmadja, G. H. Mckinley and J. J. Cooper-White, *Phys. Fluids*, 2006, **18**, 043101.
43 J. P. Rothstein and G. H. McKinley, *J. Rheol.*, 2002, **46**, 1419–1443.
44 B. Steinhaus, A. Q. Shen and R. Sureshkumar, *Phys. Fluids*, 2007, **19**, 073103.

45 P. E. Arratia, J. P. Gollub and D. J. Durian, *Phys. Rev. E: Stat., Nonlinear, Soft Matter Phys.*, 2008, **77**, 036309.
46 S. Quake and A. Scherer, *Science*, 2000, **290**, 1536.
47 S. Sia and G. Whitesides, *Electrophoresis*, 2003, **24**, 3563.
48 S. Gerashchenko and V. Steinberg, *Phys. Rev. E: Stat., Nonlinear, Soft Matter Phys.*, 2008, **78**, 040801.
49 R. B. Bird and, *et al.*, *Dynamics of Polymeric Liquids: Fluid Mechanics*, Wiley, New York, 2nd edn, 1987, vol. 1.
50 R. G. Larson, *The Structure and Rheology of Complex Fluids*, Oxford University Press, New York, 1999.
51 M. C. Sostarecz and A. Belmonte, *Phys. Fluids*, 2004, **16**, 67–70.
52 M. S. N. Oliveira and G. H. McKinley, *Phys. Fluids*, 2005, **17**, 071704.
53 P. E. Arratia, L.-A. Cramer, J. P. Gollub and D. J. Durian, *New J. Phys.*, 2009, **11**, 115006.
54 C. Wagner, Y. Amarouchene, D. Bonn and J. Eggers, *Phys. Rev. Lett.*, 2005, **95**, 164504.
55 P. E. Arratia, C. C. Thomas, J. Diorio and J. P. Gollub, *Phys. Rev. Lett.*, 2006, **96**, 144502.
56 J. P. Rothstein, *J. Rheol.*, 2003, **47**, 1227–1247.
57 J. Xu, *et al.*, *Rheol. Acta*, 2005, **44**, 537–562.
58 R. F. Hariadi and B. Yurke, *Phys. Rev. E: Stat., Nonlinear, Soft Matter Phys.*, 2010, **82**, 046307.
59 M. T. Islam, S. A. Vanapalli and M. J. Solomon, *Macromolecules*, 2004, **37**, 1023–1030.
60 J. Meadows, P. A. Williams and J. C. Kennedy, *Macromolecules*, 1995, **28**, 2683–2692.
61 Y. Liu and V. Steinberg, *Europhys. Lett.*, 2010, **90**, 44002.
62 M. D. Wang, *et al.*, *Biophys. J.*, 1997, **72**, 1335–1346.
63 T. R. Strick, *et al.*, *Science*, 1996, **271**, 1835–1837.
64 G. C. Randall, K. M. Schultz and P. S. Doyle, *Lab Chip*, 2006, **6**, 516–525.
65 H.-R. Jiang and M. Sano, *Appl. Phys. Lett.*, 2007, **91**, 154104.
66 M. D. Graham, *Annu. Rev. Fluid Mech.*, 2011, **43**, 273–298.

